Ammonothermal Synthesis of a Mesoporous Si−Ti−N Composite Material from a Single-Source Precursor

Fei Cheng,* Stephen M. Kelly, Stephen Clark, Nigel A. Young, Stephen J. Archibald, and John S. Bradley

Department of Chemistry, The University of Hull, Cottingham Road, Hull, HU6 7RX, UK

Frédéric Lefebvre

Laboratoire de Chimie Organométallique de Surface, 43 Bd du 11 Novembre 1918, 69616, Villeurbanne Cedex, France

Received June 28, 2005. Revised Manuscript Received August 30, 2005

The preparation and structure of the novel compound bis(dimethylamino)silylamino-μ-bis[(dimethylamino)silylimino]titanium $\{Ti[NHSi(NMe_2)_3]_2[\mu\text{-}NSi(NMe_2)_3]\}_2$, **1**, are reported. Ammonolysis of compound **1** in an autoclave at 160 °C gave a mesoporous silicon titanium imide powder, **2**, with a high surface area and narrow pore size distribution. A mesoporous Si−Ti−N composite material was obtained after pyrolysis of powder **2** under NH_3 flow at 1000 °C. The BET surface area is 163 $m^2\ g^{-1}$, and the average pore diameter is 71 Å. The influence of the pyrolysis temperature on the porosity of the product is also discussed on the basis of FTIR and nitrogen physisorption analyses.

Introduction

Micro- and mesoporous solids with a high effective surface area and a narrow pore size distribution have attracted considerable attention because of their potential selective property in applications in catalysis, catalyst supports, gas filters, and sensors.[1,2] The overwhelming majority of these micro- and mesoporous solids are oxide materials.[3] In recent years considerable efforts have been devoted to preparing micro- and mesoporous non-oxide solids analogous to the wide range of porous oxide materials. Bradley and coworkers reported for the first time the preparation of microporous silicon imido nitrides by the pyrolysis reactions of polysilazanes.[4−6] High surface area mesoporous silicon imido nitrides were also synthesized recently by the ammonolysis of silicon tetrachloride in organic solvents.[7] Mesoporous silicon nitride materials with narrow pore size distributions were obtained from silicon halides and ammonia in organic solvents at room temperature and subsequent dehalogenation at high temperature.[8] In addition, several nonoxidic sol−gel processes have been developed more recently to prepare novel porous non-oxide materials including Si_3N_4, BN, Si_3N_4−BN, and Si_3N_4−AlN.[2,9−13]

We recently reported the preparation of tris(dimethylamino)silylamine $H_2NSi(Me_2N)_3$ (TDSA) and lithium tris(dimethylamino)silylamide $LiHNSi(Me_2N)_3$.[14,15] TDSA has two immediate areas of impact. First, the presence of the labile $(Me_2N)_3Si$ groups makes the controlled nonaqueous ammonolysis of TDSA possible so that TDSA can be converted into a high surface area, porous silicon diimide gel.[14] Pyrolysis of the silicon diimide gel under NH_3 flow gave mesoporous silicon nitride with a high surface area and a narrow pore size distribution, thus establishing a novel nonoxidic sol−gel process to porous silicon nitride.[9] Second, due to the presence of reactive $SiNH_2$ or SiNHLi groups, TDSA and its lithium salt are versatile reaction intermediates in the preparation of a wide range of multinary silylamides that are potentially important single-source precursors to multinary silicon-based nitride ceramics. The synthetic strategy we have adopted uses TDSA, or its lithium salt, as a starting material to assemble single-source precursor molecules containing, in addition to peripheral $Si(NMe_2)_3$

* To whom correspondence should be addressed. E-mail: f.cheng@hull.ac.uk. Tel: +44-1482 465419. Fax: +44-1482 466410.

(1) Thomas, J. M.; Thomas, W. J. *Heterogeneous Catalysis*; VCH: Weinheim, 1997.
(2) Farrusseng, D.; Schlichte, K.; Spliethoff, B.; Wingen, A.; Kaskel, S.; Bradley, J. S.; Schüth, F. *Angew. Chem., Int. Ed.* **2001**, *40*, 4204.
(3) LePage, J. F. In *Handbook of Heterogeneous Catalysis*; Ertl, G., Knözinger, H., Weitkamp, J., Eds.; Wiley VCH: Weinheim, 1997; Vol. 1.
(4) Dismukes, J. P.; Johnson, J. W.; Bradley, J. S.; Milar, J. M. *Chem. Mater.* **1997**, *9*, 699.
(5) Bradley, J. S.; Vollmer, O.; Rovai, R. *Adv. Mater.* **1998**, *10*, 938.
(6) Vollmer, O.; Lefebvre, F.; Bradley, J. S. *J. Mol. Catal. A.* **1999**, *146*, 87.
(7) Kaskel, S.; Farrusseng, D.; Schlichte, K. *Chem. Commun.* **2000**, 2481.
(8) Kaskel, S.; Schlichte, K.; Zibrowius, B. *Phys. Chem. Chem. Phys.* **2002**, *4*, 1675.
(9) Cheng, F.; Clark, S.; Kelly, S. M.; Bradley, J. S.; Lefebvre, F. *J. Am. Ceram. Soc.* **2004**, *87*, 1413.
(10) Völger, K. W.; Kroke, E.; Gervais, C.; Saito, T.; Babonneau, F.; Riedel, R.; Iwamoto, Y.; Hirayama, T. *Chem. Mater.* **2003**, *15*, 755.
(11) (a) Lindquist, D. A.; Borek, T. T.; Kramer, S. J.; Narula, C. K.; Johnston, G.; Schaeffer, R.; Smith, D. M.; Paine, R. T. *J. Am. Ceram. Soc.* **1990**, *73*, 757. (b) Janik, J. F.; Ackerman, W. C.; Paine, R. T.; Hua, D. W.; Maskara, A.; Smith, D. M. *Langmuir* **1994**, *10*, 514.
(12) Cheng, F.; Toury, B.; Lefebvre, F.; Bradley, J. S.; Lefebvre, F. *Chem. Commun.* **2003**, 242.
(13) Cheng, F.; Kelly, S. M.; Lefebvre, F.; Clark, F.; Supplit, R.; Bradley, J. S. *J. Mater. Chem.* **2005**, *15*, 772.
(14) Rovai, R.; Lehmann, C. W.; Bradley, J. S. *Angew. Chem., Int. Ed.* **1999**, *38*, 2036.
(15) Bradley, J. S.; Cheng, F.; Archibald, S. J.; Supplit, R.; Rovai, R.; Lehmann, C. W.; Krüger, C.; Lefebvre, F. *J. Chem. Soc,. Dalton Trans.* **2003**, 1846.

10.1021/cm051401m CCC: $30.25 © 2005 American Chemical Society
Published on Web 10/06/2005

groups, Si−N−M backbones (M = Al, B, Ti, Zr, etc.). In such compounds each of the ceramogenic metal centers is in an exclusively MN_n enviroment. Based on this idea single-source precursor molecules $B[NHSi(NMe_2)_3]_3$,[12] $B_3[NHSi(NMe_2)_3]_3N_3H_3$,[16,17] $(NMe_2)B_3[NHSi(NMe_2)_3]_2N_3H_3$,[17] and $(C_4H_8O)Al[HNSi(NMe_2)_3]_3$[15] have been successfully prepared. Three mesoporous variants of silicon boron nitride with different molar ratios and one silicon aluminum nitride were obtained from these precursors by a nonaqueous ammonolytic sol−gel process.[12,13,17] Preliminary results of investigations of new uses of the silicon boron nitride ceramics indicate that they act as efficient selective gas filters in solid-state gas sensor applications.[18]

Much work has been reported on the preparation of silicon titanium nitride powders by pyrolysis of polymers or oligomers which contain Si−N and Ti−N bonds.[19] Silicon titanium nitride coatings or layers are prepared mainly by chemical vapor deposition (CVD).[20,21] These silicon titanium nitride powders and layers are typically produced in dense forms, which can be used as structural and/or wear-resistant materials due to their high hardness and creep resistance.[22] Our interest is to develop new micro- and mesoporous non-oxide materials with high surface area accessible for applications in heterogeneous catalysis. Transition metal nitrides are known as materials with catalytic acitivities comparable to noble metals such as platinum or palladium.[23,24] Silicon nitride offers potential advantages as a catalyst support, particularly in high-temperature processes and/or chemically harsh conditions,[25,26] because of its unique combination of superior high-temperature mechanical properties and resistance to oxidation.[27] The combination of catalytically active titanium nitride with mechanically and chemically stable silicon nitride is beneficial for applications in high-temperature catalysis. Although Jansen and co-workers described a sol−gel route in an ammono system to prepare amorphous silicon titanium nitride using polymeric titanosilazane as starting material, neither a porous structure nor a surface area for the product was reported. To our knowledge, no research on the preparation of mesoporous Si−Ti−N composites with high surface area has been reported to date.

In this paper, we report the preparation of a novel dimeric titanium silylamide precursor, i.e, bis(dimethylamino)silylamino-μ-bis[(dimethylamino)silylimino]titanium $\{Ti[NHSi(NMe_2)_3]_2[\mu\text{-}NSi(NMe_2)_3]\}_2$, **1,** and its conversion into a mesoporous Si−Ti−N ceramic with high surface area and narrow pore size distribution. The new molecule **1** was prepared by reaction of titanium tetrachloride ($TiCl_4$) with lithium tris(dimethylamino)silylamide $(Me_2N)_3SiNHLi$. Although many silylaminotitanium precursors with a $(Ti-N)_2$ ring have been reported,[19c,28−31] only $[N(Si(NMe_2)_3)(Ti(NMe_2)_2)]_2$, which was obtained by thermolysis of $N(B(NMe_2)_2)(Si(NMe_2)_3)(Ti(NMe_2)_3)$, is a structurally characterized dimeric titanium silylamide in which both titanium atoms are in a tetrahedral TiN_4 coordination arrangement.[19c] Since molecule **1** is insoluble in common solvents, porous Si−Ti−N ceramic powder was prepared by a new ammonothermal process instead of our well-developed nonaqueous sol−gel process.

Experimental Section

General Comments. All procedures were performed under an anhydrous nitrogen atmosphere using standard Schlenk techniques or in a nitrogen-filled glovebox. The solvents, pentane and tetrahydrofuran (THF), were freshly distilled from sodium/benzophenone prior to use. Titanium chloride ($TiCl_4$) and liquified ammonia were obtained from Aldrich and Energas LTD, respectively. Lithium tris(dimethylamino)silylamide $LiHNSi(Me_2N)_3$ was prepared according to a previously reported procedure.[15] Fourier transform infrared spectra were recorded on a Nicolet Magna-500 FTIR spectrometer. ^{29}Si and ^{13}C cross-polarization (CP) NMR spectra with magic-angle spinning (MAS) were obtained with a Bruker DSX-300 spectrometer operating at frequencies of 59.6 and 75.5 MHz, respectively, with tetramethylsilane (TMS) as a reference. Nitrogen adsorption isotherms were obtained at 77 K using a Micromeretics Tristar 3000 instrument, and surface area was determined from BET analysis. The amounts of silicon and titanium in the products were determined by an inductively coupled Perkin-Elmer plasma 40 emission ICP instrument. X-ray powder diffraction analysis was carried out using a SIEMENS D5000 Instrument. Transmission electron microscopy (TEM) was performed on a JEOL 2011 electron microscope operating at an accelerating voltage of 120 kV. The sample was prepared using carbon-coated copper grids. One drop of an ethanol suspension of the sample was placed on the carbon-coated grid using a microsyringe. Titanium K-edge XAFS spectra were collected in transmission mode at ca. 80 K at the Daresbury Laboratory Synchrotron Radiation Source (2 GeV, ca. 180 mA) on station 7.1 using a sagittally focusing Si(111) double crystal monochromator. Harmonic removal was obtained using a mirror and detuning the monochromator to 70%. The data were

(16) Cheng, F.; Toury, B.; Archibald, S. J.; Bradley, J. S. *J. Organomet. Chem*. **2002**, *657*, 71.
(17) Cheng, F.; Archibald, S. J.; Clark, S.; Toury, B.; Kelly, S. M.; Bradley, J. S.; Lefebvre, F. *Chem. Mater.* **2003**, *15*, 4651.
(18) Baumbach, M.; Schütze, A.; Cheng, F.; Kelly, M. S.; Delprat, H.; Parret, F.; Menini, P.; Soulantica, K.; Chaudret, B.; Maisonnat, A. *Proc. IEEE Sensors 2004*, in press.
(19) (a) Hapke, J.; Ziegler, G. *Adv. Mater*. **1995**, *7*, 380. (b) Hering, N.; Schreiber, K.; Riedel, R.; Lichtenberger, O.; Woltersdorf, J. *Appl. Organomet. Chem.* **2001**, *15*, 879. (c) Wagner, O.; Jansen, M. *Z. Anorg. Allg. Chem.* **1994**, *620*, 366. (d) Engering, J.; Jansen, M. *Z. Anorg. Allg. Chem.* **2003**, *629*, 913. (e) Löffelholz, J.; Engering, J.; Jansen, M. *Z. Anorg. Allg. Chem.* **2000**, *626*, 963. (f) Liu, X.; Wu, Z.; Cai, H.; Yang, Y.; Chen, T.; Vallet, C. E.; Zuhr, R. A.; Beach, D. B.; Peng, Z.; Wu, Y.; Concolino, T. E.; Rheingold, A. L.; Xue, Z. *J. Am. Chem. Soc.* **2001**, *123*, 8011.
(20) Lauro, G.; Hillel, R.; Sibieude, F. *Chem. Vap. Deposition* **1998**, *4*, 247.
(21) Amato-Wierda, C. C.; Norton, E. T., Jr.; Wierda, D. A. *Chem. Mater*. **1999**, *11*, 2775.
(22) Oyama, S. T. *Transition Metal Carbides and Nitrides*; Chapman & Hall: London, 1996.
(23) Ertl, G.; Knözunger, H.; Wertkamp, J. *Handbook of Heterogeneous Catalysis, Vol. 1;* VCH: Weinheim, 1997.
(24) Kaskel, S.; Schlichte, K.; Kratzke, T. *J. Mol. Catal*. **2004**, *208*, 291.
(25) Méthivier, C.; Massardier, J.; Bertolini, J. C. *Appl. Catal., A* **1999**, *182*, 337.
(26) Hullmann, D.; Wendt, G.; Šingliar, U.; Ziegenbalg, G. *Appl. Catal. A* **2002**, *225*, 261.
(27) Narula, C. K. *Ceramic Precursor Technology and Its Applications*; Marcel Dekker: New York, 1995.
(28) Alcock, N. W.; Butler, M. P.; Willey, G. R. *Chem. Commun*. **1974**, 627.
(29) Alcock, N. W.; Butler, M. P.; Willey, G. R. *J. Chem. Soc., Dalton Trans*. **1976**, 707.
(30) Ovchinnikov, Yu. E.; Ustinov, M. V.; Igonin, V. A.; Struchkov, Yu. T.; Kalikhman, I. D.; Voronkov, M. G. *J. Organomet. Chem*. **1993**, *461*, 75.
(31) Cummins, C. C.; Schaller, C. P.; Duyne, G. D. V.; Wolczansk, P. T.; Chan, A. W. E.; Hoffman, R. *J. Am. Chem. Soc*. **1991**, *113*, 2985.

calibrated using the first maximum of the first derivative of a Ti foil (4966.0 eV) placed between I_t and I_{cal} ion chambers. Background subtraction was carried out using PAXAS[32] by fitting the pre-edge to a quadratic polynomial and post-edge using either high-order polynomials or splines. The data were fitted using EXCURV98.[33] For multiple scattering pathways the cluster formalism was employed.

Synthesis of Bis(dimethylamino)silylamino-μ-bis[(dimethylamino)silylimino]titanium, {Ti[NHSi(NMe$_2$)$_3$]$_2$[μ-NSi(NMe$_2$)$_3$]}$_2$, 1. A solution of $TiCl_4$ (0.86 g, 4.5 mmol) in pentane (10 mL) was added to a suspension of $LiHNSi(Me_2N)_3$ (3.3 g, 18.3 mmol) in 40 mL of pentane. After 15 h of stirring at room temperature, the resulting precipitate of lithium chloride was removed by filtration, and the filtrate was evaporated under reduced pressure to give a brown oil. After 2 weeks at room temperature the oil transformed into yellow crystals **1,** which were then isolated by filtration and washed with pentane. (Yield: 43.3%**).** IR (KBr, cm^{-1}): 3250 (w) (ν(NH)); 2973 (s), 2874 (s), 2835 (s), 2782 (s), ($\nu(CH_3)$); 1177 (s); 986 (s).

For the crystal structure determination of **1** a crystal was mounted on a glass fiber using perfluoropolyether oil and transferred to a Stöe IPDS II imaging plate diffractometer equipped with an Oxford Cryosystems 700 series cooling system. The data were collected using graphite-monochromated Mo Kα radiation ($\lambda = 0.71073$) at 150 K. Absorption correction was not applied. The structure was solved by direct methods (SHELXS 97)[34] and refined by full-matrix least-squares on F^2 using SHELXL 97.[35] All non-hydrogen atoms were refined anisotropically. Hydrogen atoms were placed in idealized positions.

Ammonolysis. The ammonothermal reaction was carried out at 160 °C in a stainless steel Parr autoclave fitted with a pressure gauge. The autoclave was charged with compound **1** (3.4 g) in a glovebox and then ammonia (6 mL) was condensed into the autoclave at −78 °C. The autoclave was sealed and heated to 160 °C in an oil bath reaching a pressure of 1.5 MPa. After 24 h the autoclave was cooled to room temperature, flushed with nitrogen for 0.5 h, and then evacuated under reduced pressure for 1 h to remove ammonia and resultant dimethylamine. The brown solid (1.4 g), **2**, was collected in a glovebox. ^{29}Si CP-MAS NMR: δ −39 ppm; ^{13}C CP-MAS NMR: δ 37.9 ppm. IR (neat, cm^{-1}): 3322 (m, ν(NH)); 2993 (w), 2921 (w), 2855 (w), 2795 (w) (ν(CH)); 1558 (w, $\delta(NH_2)$); 1177 (s, δ(N−C) and δ(NH)); 929, 920 (s, ν(Si−N)).

Pyrolysis. The ammonolyzed product **2** was pyrolyzed in a tube furnace. About 0.5 g of **2** was placed in an Al_2O_3 boat, which was then introduced into a quartz tube in a glovebox. The ammonolyzed product was heated to 200 °C with a ramp rate of 5 °C min^{-1}, held at 200 °C for 2 h, and then heated at 1000 °C for 2 h under NH_3 flow.

Results and Discussion

Synthesis of Precursor Molecule 1. The reaction of 4 equiv of lithium tris(dimethylamino)silylamide $LiHNSi(Me_2N)_3$[15] with titanium tetrachloride $TiCl_4$ in pentane (eq 1) gave a brown oil. ^{1}H NMR and FTIR analyses showed that the oil is a mixture of the tetrakis[tris(dimethylamino)silylamide]titanium complex (Ti[NHSi(NMe$_2$)$_3$]$_4$), TDSA, and a small amount of byproducts. This titanium silylamide is not stable and will decompose into crystalline products

$$TiCl_4 + 4LiHNSi(NMe_2)_3 \xrightarrow{\text{pentane}} Ti[NHSi(NMe_2)_3]_4 + 4LiCl \quad (1)$$

$$2Ti[NHSi(NMe_2)_3]_4 \rightarrow \{Ti[NHSi(NMe_2)_3]_2[NSi(NMe_2)_3]\}_2 + 2H_2NSi(NMe_2)_3 \quad (2)$$

{Ti[NHSi(NMe$_2$)$_3$]$_2$[μ-NSi(NMe$_2$)$_3$]}$_2$ (eq 2). The formation of $H_2NSi(NMe_2)_3$ confirms the decomposition of Ti[NHSi(NMe$_2$)$_3$]$_4$.

The crystalline product **1** of this reaction was not characterized by solution NMR due to insolubility in common solvents. IR analysis shows a weak absorption at 3276 cm^{-1} which can be assigned to ν(NH) of the TiNHSi groups (Figure 1). The strong absorption at 929 cm^{-1} can be ascribed to ν(Si−N) of $SiNMe_2$ groups. The results of elemental analysis were unsatisfactory because the crystalline product **1** is very air-sensitive.

The molecular structure of compound **1** was determined by single-crystal X-ray diffraction analysis (Table 1). A view of the molecule is shown in Figure 2 and selected bond lengths and angles are collected in Table 2. The molecule

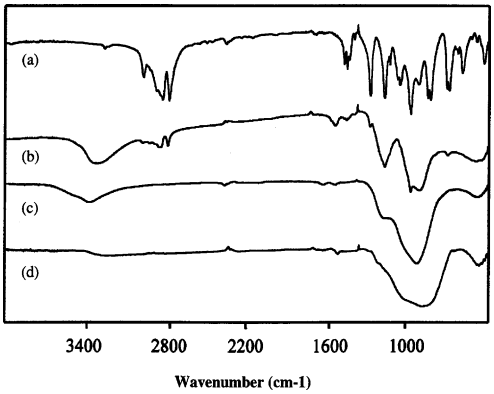

Figure 1. IR spectra of (a) precursor molecule **1,** (b) the ammonolysis product **2,** (c) the pyrolyzed product from **2** under NH_3 flow at 600 °C, and (d) the pyrolyzed product from **2** under NH_3 flow at 1000 °C. The spectra were obtained by KBr disk except for (a) which was characterized by liquid film.

Table 1. Crystal Data for Compound 1

formula	$C_{36}H_{112}N_{24}Si_6Ti_2$
M	1145.84
crystal system	monoclinic
space group	$P2_1/n$
a/Å	13.064(2)
b/Å	12.7709(14)
c/Å	19.980(4)
a/deg	90
β/deg	103.97(13)
γ/deg	90
volume/Å^3	3234.9(8)
Z	2
crystal size/mm	0.23 0.21 0.08
T/K	150(2)
reflections collected	48314
unique reflections (R_{int})	13968 (0.1515)
restraints/parameters	0/325
goodness of fit on F^2	0.577
R1, wR2 [$I > 2\sigma(I)$]	0.0428, 0.0611
R1, wR2 (all data)	0.2142, 0.0794

(32) Binsted, N. *PAXAS*, Program for the analysis of X-ray absorption spectra; University of Southampton: U.K., 1988.
(33) Binsted, N. *EXCURV98*, CCLRC Daresbury Laboratory Computer Program; CCLRC, Daresbury Laboratory: U.K., 1998.
(34) Sheldrick, G. M. *SHELXS-97*, Program for structure solution; University of Göttingen: Göttingen, Germany, 1997.
(35) Sheldrick, G. M. *SHELXL-97*: Program for the Refinement of Crystal Structures; University of Göttingen: Göttingen, Germany, 1997.

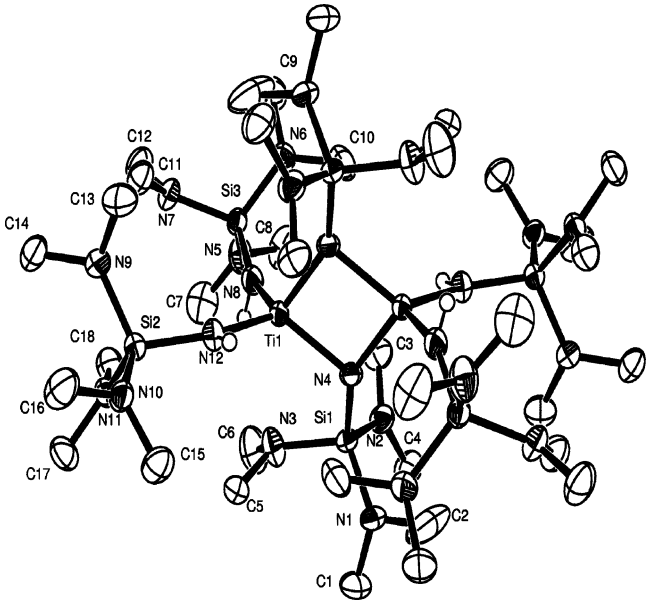

Figure 2. ORTEP[36] plot of the crystal structure of compound **1**. Hydrogen atoms are omitted for clarity.

Table 2. Selected Bond Distances (Å) and Angles (deg) for Compound 1

Ti(1)−N(4)	1.9894(17)	N(4*)−T1(1)−N(8)	111.56(8)
T1(1)−N(4*)	1.8797(13)	N(4*)−Ti(1)−N(12)	105.83(8)
Ti(1)−N(8)	1.9108(17)	N(4*)−Ti−N(4)	84.12(8)
Ti(1)−N(12)	1.9280(18)	N(8)−Ti(1)−N(12)	112.61(7)
Si(1)−N(4)	1.7112(18)	N(8)−Ti(1)−N(4)	118.86(8)
Si(2)−N(12)	1.71243(18)	N(12)−Ti(1)−N(4)	118.94(7)
Si(3)−N(8)	1.7076(17)	N(4*)−Ti(1)−Ti(1*)	43.52(5)
T1(1)−Ti(1*)	2.8737(8)	N(8)−Ti(1)−Ti(1*)	125.07(6)
N(4)−Ti(1*)	1.8787(17)	N(12)−Ti(1)−Ti(1*)	120.89(5)
		N(4)−Ti(1)−Ti(1*)	40.59(5)
		Si(1)−N(4)−Ti(1*)	145.93(11)
		Si(1)−N(4)−Ti(1)	113.08(8)
		Ti(1*)−N(4)−Ti(1)	95.88(8)
		Si(3)−N(8)−Ti(1)	156.27(13)
		Si(2)−N(12)−Ti(1)	148.39(10)

contains a planar four-membered Ti_2N_2 ring with a C_{2h} symmetry. The titanium atoms are coordinated in a distorted tetrahedron by two nearly planar terminal silylamindo ligands and two slightly pyramidal bridging silylimido ligands. The two endocyclic Ti−N distances are 1.99 Å, which can be ascribed to the formation of a Ti−N single bond.[29,37] The two other endocyclic Ti−N distances are both 1.879 Å, which are probably shortened by $d_\pi-p_\pi$ interactions.[19c,37] Unsymmetrically bridging imido ligands have also been observed in other dimeric transition metal amides such as $[(NSi(NMe_2)_3)(Ti(NMe_2)_2]_2$[19c] and $[(CH_3)_2(t\text{-}BuN)M]_2(\mu\text{-}t\text{-}BuN)_2$ (M = Mo, W).[38,39] The exocyclic Ti−N distances are 1.92 and 1.91 Å, respectively.

The mean internal ring angles at titanium (84.12(8)°) are smaller than that at nitrogen (95.88(8)°), which is similar to those reported for $[(NSi(NMe_2)_3)Ti(NMe_2)_2]_2$ in the literature.[20] The Ti···Ti distance across the ring is 2.87 Å.

The presence of a strong pre-edge feature at 4969.4 eV in the Ti K-edge XANES spectrum of **1** (Figure 3a) is

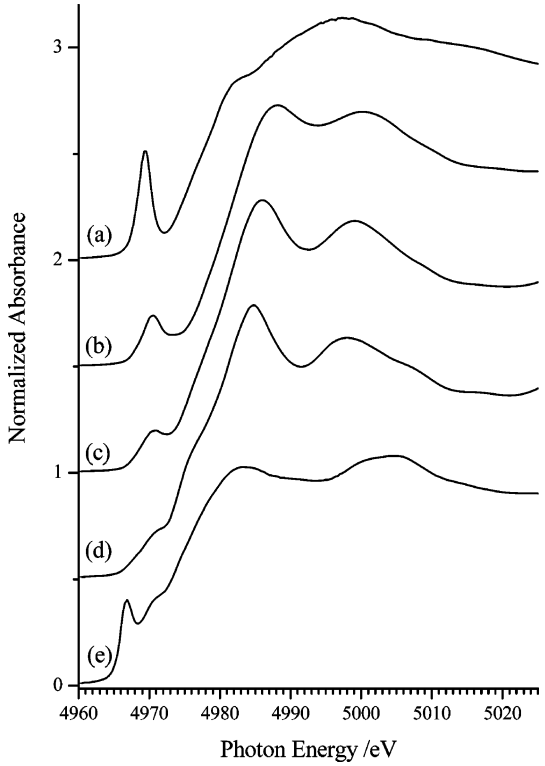

Figure 3. Ti K-edge XANES spectra of (a) **1**, (b) **2**, (c) **3**, (d) TiN, and (e) Ti.

characteristic of tetrahedral Ti geometry.[40] The Ti K-edge EXAFS (Figure 4a and Table 3) refined to values in reasonable agreement with the crystal structure, except that it was not possible to separate the different T−N distances around each Ti. In addition to the Ti...Ti bridging distance at 2.89(3) Å, a Ti...Si at 2.91(3) Å (compared to 3.091 Å in the crystal) improved the quality of the fit, but there is also a Ti...N distance at 2.932 Å in the crystal structure that could not be included on the basis of statistical significance.

Ammonolysis. The reaction of compound **1** with ammonia in an autoclave at 160 °C gave a brown solid **2**. An ideal reaction can be expressed as eq 3.

$$\{Ti[NHSi(NMe_2)_3]_2[NSi(NMe_2)_3]\}_2 + 18NH_3 \rightarrow 2TiSi_3(N)(NH)_2(NH_2)_9 + 18HNMe_2 \quad (3)$$

The IR spectrum of compound **2** (Figure 1b) shows a broad ν(N−H) band centered at 3322 cm^{-1} and a low-intensity band at 1591 cm^{-1} (due to the presence of NH_2), suggesting that the NH groups are present with different environments, such as Si−NH−Si, Si−NH−Ti and $SiNH_2$. Compared to the IR spectrum of precursor compound **1**, the low intensity of the ν(CH) bands from 2795 to 2993 cm^{-1} indicates that most of the dimethylamino groups have been removed in the reaction. The broad absorbance at about 1190 cm^{-1} is due to the presence of δ(N−C) and δ(N−H).[7,41] The broad band from 900 to 1005 cm^{-1} can be assigned to ν(Si−N),

(36) Farrugia, L. J. *J. Appl. Crystallogr*. **1997**, *30*, 565.
(37) Faxos, J.; Mootz, D. *Z. Anorg. Chem*. **1971**, *380*, 196.
(38) Nugent, W. A.; Harlow, R. L. *J. Am. Chem. Soc*. **1980**, *102*, 1759.
(39) Thorn, D. L.; Nugent, W. A.; Harlow, R. L. *J. Am. Chem. Soc*. **1981**, *103*, 357.
(40) (a) Farges, F.; Brown, G. E.; Rehr, J. J. *Geochim. Cosmochim. Acta* **1996**, *60*, 3023. (b) Mountjoy, G.; Pickup, D. M.; Wallidge, G. W.; Anderson, R.; Cole, J. M.; Newport, R. J.; Smith, M. E. *Chem. Mater*. **1999**, *11*, 1253. (c) Mountjoy, G.; Pickup, D. M.; Wallidge, G. W.; Cole, J. M.; Newport, R. J.; Smith, M. E. *Chem. Phys. Lett*. **1999**, *304*, 150. (d) Sankar, G.; Thomas, J. M.; Catlow, C. R. A.; Barker, C. M.; Gleeson, D.; Kaltsoyannis, N. *J. Phys. Chem. B* **2001**, *105*, 9028.

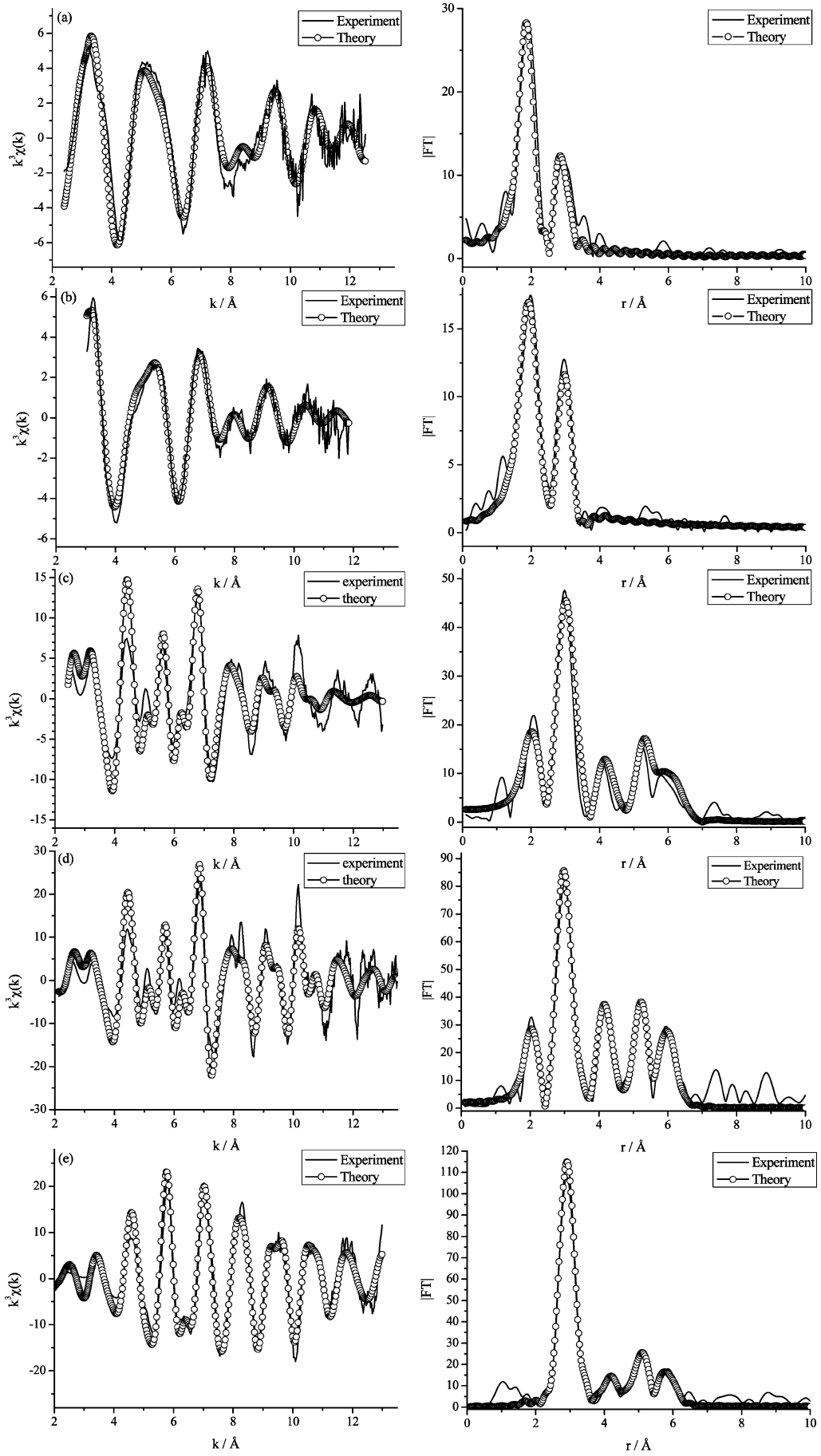

Figure 4. Ti K-edge EXAFS and FTs of (a) **1**, (b) **2**, (c) **3**, (d) TiN, and (e) Ti.

Table 3. Refined EXAFS Parameters for 1, 2, 3, TiN, and Ti

1	XRD[a] *r*/Å	EXAFS[a] *r*/Å[b]	$2\sigma^2$/Å^2 [c]	**2**	EXAFS[a] *r*/Å[b]	$2\sigma^2$/Å^2 [c]	**3**	EXAFS[a] *r*/Å[b]	$2\sigma^2$/Å^2 [c]
$Ti-N_4$	1.928[d]	1.910(6)	0.016(1)	$Ti-N_4$	1.974(7)	0.026(1)	$Ti-N_6$	2.117(10)	0.035(6)
Ti−Ti	2.874	2.887(14)	0.006(2)	Ti−Ti	2.999(10)	0.014(2)	$Ti-Ti_{12}$	3.026(7)	0.028(2)
Ti−Si	3.091	2.914(43)	0.019(16)	Ti−Si	2.759(24)	0.030(9)	$Ti-Ti_6$	4.234[e]	0.041(5)
							$Ti-Ti_{24}$	5.256(18)	0.032(4)
							$Ti-Ti_{12}$	6.052[f]	0.037(6)
E_f[g]		−9.9(5)			1.1(7)			2.1(6)	
R[h]		34.8%			26.0%			54.0%	

TiN	XRD[i] *r*/Å	EXAFS[a] *r*/Å[b]	$2\sigma^2$/Å^2 [c]	**Ti**	XRD[j] *r*/Å	EXAFS[a] *r*/Å[b]	$2\sigma^2$/Å^2 [c]
$Ti-N_6$	2.119	2.110(6)	0.021(5)	$Ti-Ti_6$	2.894	2.885(16)	0.011(2)[k]
$Ti-Ti_{12}$	2.997	2.995(5)	0.016(1)	$Ti-Ti_6$	2.951	2.944(16)	0.011(2)[k]
$Ti-Ti_6$	4.238	4.220[e]	0.019(2)	$Ti-Ti_6$	4.133	4.125(20)	0.023(5)
$Ti-Ti_{24}$	5.190	5.203(12)	0.017(2)	$Ti-Ti_2$	4.679	4.666(70)	0.020(18)
$Ti-Ti_{12}$	5.993	5.990[f]	0.021(3)	$Ti-Ti_{12}$	5.079	5.100(11)	0.014(2)
				$Ti-Ti_6$	5.111	5.189(326)	0.088(176)
				$Ti-Ti_{12}$	5.532	5.759(69)	0.036(32)
				$Ti-Ti_6$	5.902	5.888[l]	0.022(6)
E_f[g]		−3.1(6)				−12.8(4)	
R[h]		54.2%				30.8%	

[a] This work. [b] EXAFS errors on well-defined interatomic distances are estimated to be ±1%. [c] Debye−Waller factor. [d] Average of four Ti−N in Table 2. [e] Constrained to be twice r_{Ti-N} of first shell. [f] Constrained to be twice r_{Ti-Ti} in second shell. [g] Refined parameter to reflect difference between experimental and calculated Fermi level. [h] Measure of goodness of fit. [i] Reference: Schoenberg, N. *Acta Chem. Scand.* **1954**, *8*, 213. [j] Reference: Spreadborough, J.; Christian, J. W. *Proc. Phys. Soc. London* **1959**, *74*, 609. [k] Constrained to be equal. [l] Constrained to be twice r_{Ti-Ti} in second shell.

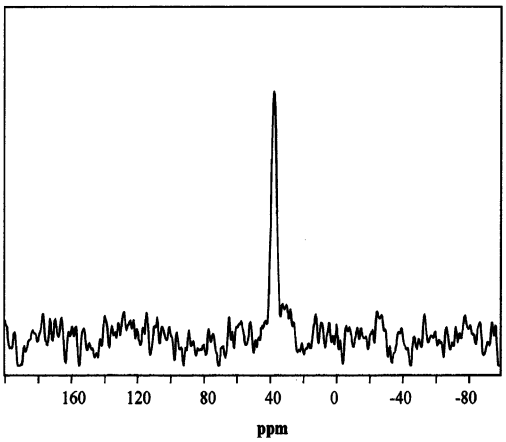

Figure 5. ^{13}C CP MAS NMR of ammonolyzed product **2**.

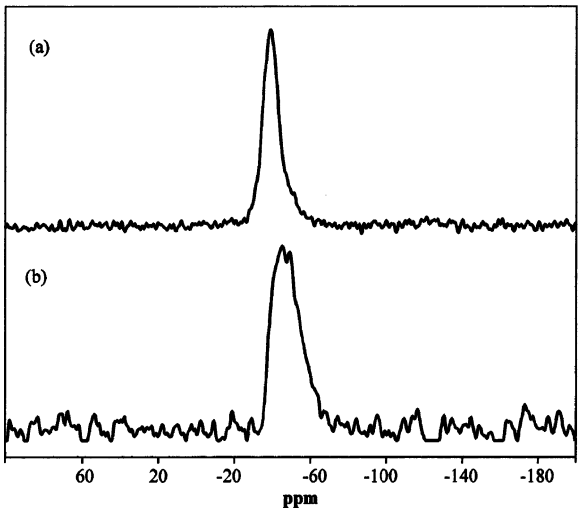

Figure 6. ^{29}Si CP MAS NMR of (a) ammonolyzed product **2** and (b) pyrolyzed product from **2**.

in which absorption at 929 cm^{-1} should be from $SiNMe_2$ groups of compound **1**.[41] The ^{13}C CP-MAS NMR spectra shows a single resonance at 37.9 ppm due to the presence of $Si(NMe_2)_x$ (Figure 5), consistent with the IR result. ^{29}Si CP-MAS NMR spectrum (Figure 6a) exhibits a single resonance at −39 ppm, indicating the formation of SiN_4 environments in which silicon is mainly coordinated to $(NH)_x$ groups.[5,8]

The shift to higher energy and reduction in intensity of the pre-edge feature at 4970.6 eV in the Ti K-edge XANES of the ammonolysis product **2** (Figure 3b) is consistent with an increase in coordination number around the Ti.[40] The Ti K-edge EAXFS of **2** is different from that of **1**, and in particular the FT indicates that there is a change in the relative intensity of the Ti−N and Ti...Ti shells. The detailed modeling used the parameters from **1** as a starting point and indicated that the average Ti−N bond length has increased from 1.91(2) Å in **1** to 1.97(2) Å in **2**. The Debye−Waller factor has increased on ammonolysis, indicating an increase in local disorder around the Ti. This is probably due to both a variety of species present and a spread of distances in each case. The average Ti...Ti distance also increases from 2.89(3) to 3.00(3) Å on ammonolysis as does the Debye−Waller factor associated with this shell. The Ti...Si distance appears to decrease from **1** to **2**, but given that its Debye−Waller factor is now very large, this is probably not significant. Therefore, the Ti K-edge XANES and EXAFS are consistent with the loss of tetrahedral Ti sites, and their replacement by higher coordination environments, probably octahedral.

All these spectral features indicate that ammonolysis of the precursor compound **1** led to formation of a silicon titanium imide powder **2** containing residual dimethylamino groups, $Si_3Ti(N)(NH)_x(NH_2)_y(NMe_2)_z$. Nitrogen adsorption isotherms of the ammonolyzed product **2** is shown in Figure 7. The difference (hysteresis) between adsorption and desorption in the range of relative pressure between 0.4 and 0.8 indicates the presence of mesoporous material. The

(41) Nakamoto, K. *Infrared and Roman Spectra of Inorganic and Coordination Compounds*; John Wiley & Sons: New York, 1997.

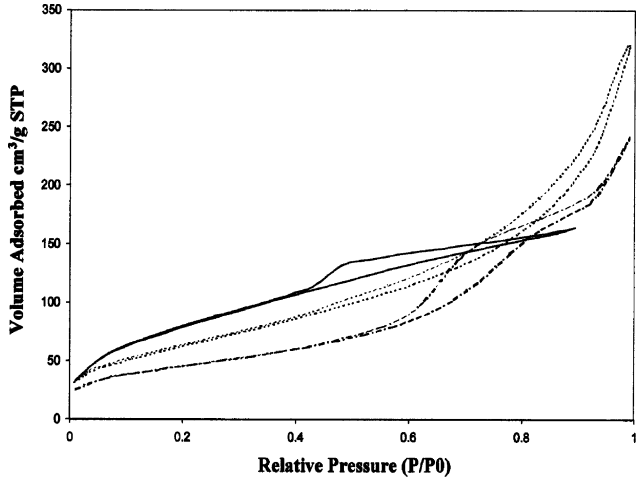

Figure 7. Nitrogen adsorption and desorption isotherms of ammonolyzed product **2** (−), pyrolyzed product at 600 °C (···), and pyrolyzed product at 1000 °C (---).

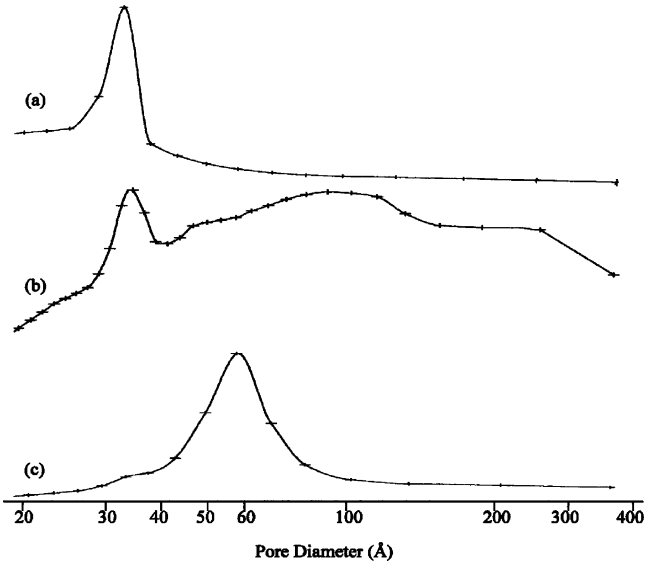

Figure 8. Pore size distribution of (a) ammonolyzed product **2**, (b) pyrolyzed product at 600 °C, and (c) pyrolyzed product at 1000 °C.

surface area is 301 m^2/g and the pore size varies from 27 to 40 Å with an average pore diameter of 33 Å (Figure 8). The pore size distribution is very similar to that of silicon diimide gel prepared by catalytic ammonolysis of $H_2NSi(NMe_2)_3$.[9] The high surface area and narrow pore size distribution suggest that the imide powder **2** should have three-dimensional networks mainly connected by Si−N(H)−Si backbones formed during the ammonolysis and condensation reactions (eqa 4−6). The presence of residual dimethylamino groups shows that the transamination reactions were not yet complete under these reaction conditions.

$$\equiv Si-NMe_2 + NH_3 \rightarrow \equiv Si-NH_2 + HNMe_2 \quad (4)$$

$$\equiv Si-NH_2 + Me_2N-Si\equiv \rightarrow \equiv Si-NM-Si\equiv + HNMe_2 \quad (5)$$

$$2\equiv Si-NH_2 \rightarrow \equiv Si-NH-Si\equiv + NH_3 \quad (6)$$

The formation of a silicon titanium imide containing residual dimethylamino groups was further confirmed by TG-MS analysis. Thermogravimetric analysis of the solid **2** under argon shows that a continuous mass loss occurs over the full temperature range from 25 to 1000 °C (Figure 9). The ceramic yield up to 1000 °C is 68%. MS spectra coupled with TG show that the dimethylamine ($HNMe_2$) and ammonia (NH_3) evolved below 400 and 600 °C, respectively. The evolution of $HNMe_2$ and NH_3 indicates that further condensation reactions occurred during the pyrolysis as shown in eqs 5−8. At a temperature over 300 °C hydrogen is evolved, probably because of the homolytic cleavage of N−H bonds followed by H abstraction (eqs 10 and 11).[42]

$$\equiv Si-NH-Si\equiv + Me_2N-Si\equiv \rightarrow N(Si\equiv)_3 + HNMe_2 \quad (7)$$

$$\equiv Si-NH_2 + \equiv Si-NH-Si\equiv \rightarrow N(Si\equiv)_3 + NH_3 \quad (8)$$

$$2\equiv Si-NH-Si\equiv \rightarrow N(Si\equiv)_3 + \equiv Si-NH_2 \quad (9)$$

$$N-H \rightarrow N\cdot + H\cdot \quad (10)$$

$$H\cdot \xrightarrow{\text{H abstraction}} H_2 \quad (11)$$

Pyrolysis. Since pyrolysis under ammonia is a potentially useful process to reduce the carbon contamination from preceramic materials containing dialkylamino groups,[43−45] ammonolyzed product **2** was pyrolyzed under an atmosphere of ammonia. The IR spectra of the products pyrolyzed at 600 and 1000 °C are shown in Figure 1. As expected, the disappearance of the ν(CH) bands from 2795 to 2993 cm^{-1} in the IR spectrum of the pyrolyzed product at 600 °C indicates that dimethylamino groups have been removed completely. The broad ν(N−H) bands centered at 3322 cm^{-1} and δ(N−H) band at 1190 cm^{-1} suggest that a considerable amount of NH groups are present in the product. Pyrolysis at 1000 °C for 2 h gave a brown solid, **3**, with a ceramic yield of 63.5%. IR analysis shows that nearly all of the NH groups are lost, probably due to the homolytic cleavage of N−H bonds followed by H abstraction (eqs 10 and 11). The broad band centered at 940 cm^{-1} can be ascribed to ν(Si−N).[40]

The ^{29}Si CP-MAS NMR spectrum of the final product **3** shows a broad resonance at about −46 ppm (Figure 6b), consistent with the value observed for SiN_4 tetrahedra with a large distribution of different distortions.[46] Typically broad reflections for TiN are observed in the X-ray powder diffraction patterns (Figure 10), suggesting a small particle size.[48] TEM investigation (Figure 11) reveals nanometer-sized pores, but without ordered structures, which is consistent with the XRD result. ICP emission analysis shows that the molar ratio of the silicon to titanium in the final product **3** is 2.3:1, lower than that present in the ammonolyzed product **2**, suggesting that some of the Si-containing

(42) Choong Kwet Yive, N. S.; Corriu, R. J. P.; Leclercq, D.; Mutin, P. H.; Vioux, A. *Chem. Mater.* **1992**, *4*, 1263.
(43) Gordon, R. G.; Hoffman, D. M.; Riaz, U. *Chem. Mater.* **1990**, *2*, 480.
(44) Cheng, F.; Sugahara, Y.; Kuroda, K. *Chem. Lett.* **2000**, 138.
(45) Cheng, F.; Sugahara, Y.; Kuroda, K. *Bull. Chem. Soc. Jpn.* **2000**, *73*, 1299.
(46) Müller, U.; Hoffbauer, W.; Jansen, M. *Chem. Mater.* **2000**, *12*, 2341.
(47) Piskorska, E.; Lawniczak-Jablonska, K.; Demchenko, I. N.; Benko, E.; Welter, E. *J. Alloys Compd.* **2004**, *362*, 171.
(48) Powder diffraction data file, 03-065-0965 (for TiN), JCPDS International Center for Diffraction Data, Swathmore, PA, 2003.

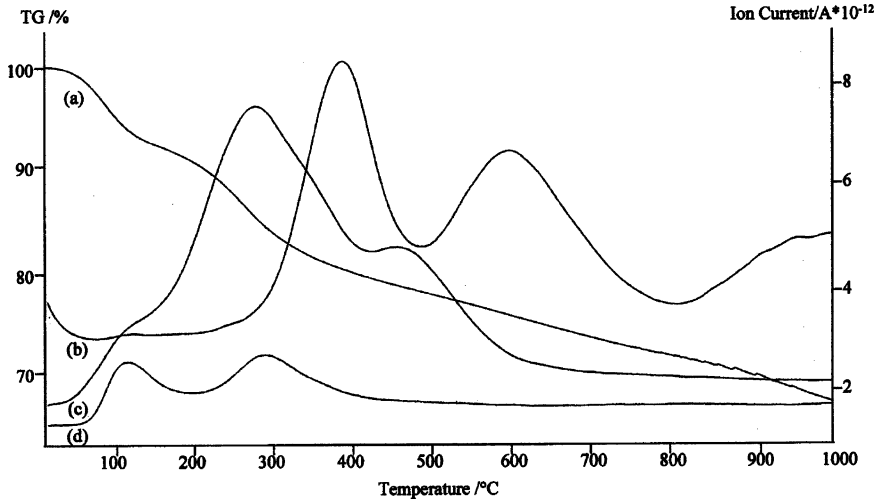

Figure 9. Thermal gravimetric (TG) analysis (a) of the ammonolyzed product **2** in Ar flow at a heating rate of 5 °C/min. The evolved gas species (b) H_2, (c) NH_3, and (d) $HNMe_2$ with $m/z = 2$, 17, and 45, respectively, were detected by a coupled mass spectrometer.

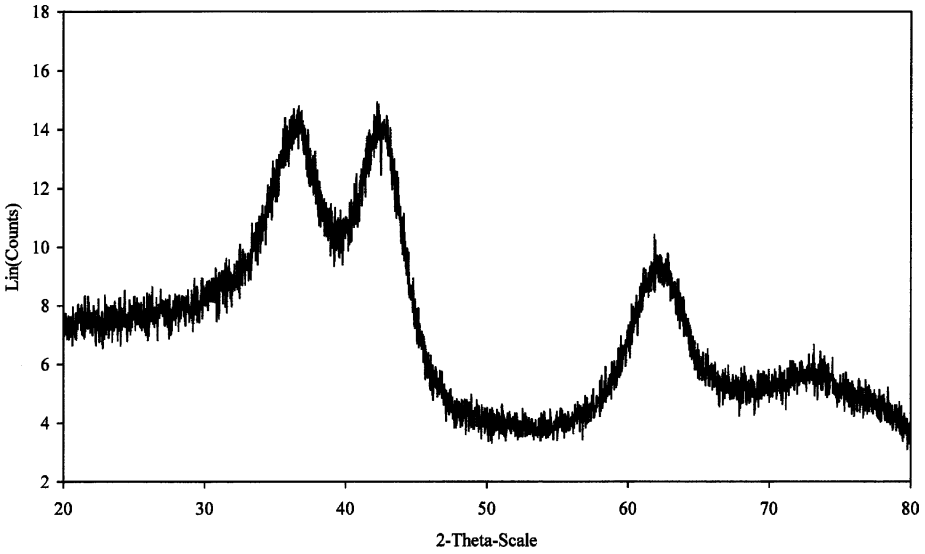

Figure 10. XRD pattern of the product pyrolyzed from ammonolyzed product **2** at 1000 °C under NH_3 flow.

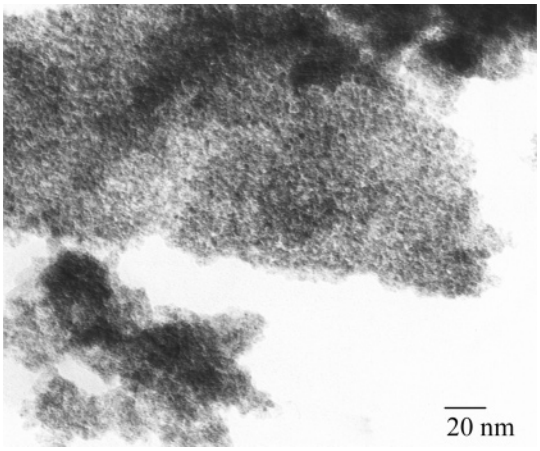

Figure 11. Transmission electron micrograph of the product pyrolyzed from ammonolyzed product **2** at 1000 °C under NH_3 flow.

species were lost during the pyrolysis. The final product **3** contained 0.11% carbon, indicating that most of the carbon in **2** has been removed during the pyrolysis.

The Ti K-edge XANES spectrum of **3** is shown in Figure 3c. The edge and post-edge structure closely resemble those of TiN (Figure 3d), and there is no evidence of the pre-edge feature found at 4966.9 eV in the spectrum of Ti metal (Figure 3e), indicating that the pyrolyzed sample most probably contains Ti in the form of TiN. The spectra of TiN and Ti are in very good agreement with those in the literature.[47] The weak pre-edge feature in the spectrum of **3** at 4970.8 eV is entirely consistent with the presence of octahedral Ti,[40] but it has more intensity than in the spectrum of TiN. As has been shown previously that tetrahedral Ti has a detection limit of about 10% in Ti K-edge XANES spectra,[41a] and that the intensity of the pre-edge feature can be slightly higher in non-centrosymmetric octahedral environments,[41a−c] this peak either could be associated with a small residual amount of tetrahedral Ti or could reflect the inherent low site symmetry found in small particles of TiN.

The Ti K-edge EXAFS and FTs of the pyrolyzed product **3**, together with those for TiN and Ti, are shown in Figure 4. The EXAFS of **3** closely resembles that of TiN, and the presence of a short Ti−N distance in the FT confirms the formation of TiN in the final ceramic. TiN has the rock-salt structure of interpenetrating fcc lattices of Ti and N. Due to the large discrepancy in atomic potential between Ti and N,

the EXAFS (and FT) is dominated by Ti−Ti interactions to such an extent that, apart from the first Ti−N shell, the remaining Ti−N interactions are not observable. This has the effect of making the FT appear similar to those observed for other fcc metals, e.g., Cu, with the addition of a short Ti−N peak. Fortunately, Ti metal adopts an hcp structure at room temperature, and the local Ti environment in this is sufficiently different (less local ordering see Table 3) from that expected for fcc Ti to be able to differentiate between them. The analysis of the Ti K-edge data for the pyrolyzed product, TiN, and Ti is also shown in Figure 4 with the parameters given in Table 3. The refinement for TiN was straightforward with one short Ti−N and the first four shells of a fcc Ti lattice, including, where appropriate, multiple scattering. The agreement between the XRD and EXAFS data is very good. The analysis of Ti metal was more awkward because of the 8 shells needed to fit the data out to 6 Å in an hcp lattice. Some of these (especially the low coordination number shells) are poorly defined, but the fit to the XRD data is very good overall. The Ti K-edge EXAFS of the pyrolyzed product is much more similar to that of TiN than Ti, and the FT confirms this with the presence of a short Ti−N. The reduction in intensity for both the EXAFS and the FT compared to the TiN data is consistent with the formation of small particles of TiN in the pyrolyzed product. When the data were fitted using the TiN parameters as a starting point, the fit shown in Figure 4 was obtained. The refined interatomic distances are all slightly longer in **3** than in the bulk TiN, and as to be expected the Debye−Waller factors are also larger, and we believe that both of these are a consequence of the presence of small TiN particles. It is illustrative to note how the Ti−N and Ti...Ti distances determined by the Ti K-edge EXAFS change from those characteristic of the discrete dimer in **1**, through intermediate values in **2**, to those very close to TiN in **3**.

Physisorption analysis (Figure 7) shows a type IV isotherm with a hysteresis loop between 0.52 and 0.93, indicating the presence of mesopores in **3**. The BET surface area is 163 $m^2\ g^{-1}$, a significant decrease from 301 $m^2\ g^{-1}$ for the ammonolyzed product **2**. The main pore size distribution (Figure 8) is from 40 to 100 Å with a small shoulder at 27−40 Å, which is from the mesopores of the ammonolyzed product **2.** On the basis of these results it can be concluded that a mesoporous Si−Ti−N composite with a high surface area and narrow pore size distribution has been obtained. The high surface area in combination with the small size distribution of nanometer-sized holes suggests that this new mesoporous material may be a very attractive ceramic with a high adsorption selectivity.

To investigate the influence of pyrolysis temperature on the porosity of the residues, the ammonolyzed product **2** was pyrolyzed at 600 °C under NH_3 flow. The nitrogen physisorption analysis results of the pyrolyzed product are showed in Figure 7 and Figure 8. The product pyrolyzed at 600 °C has a type II isotherm with a BET surface area of 233 $m^2\ g^{-1}$. Compared to ammonolyzed product **2**, a considerable amount of mesopores from 27 to 40 Å are lost and new pores, which are widely scattered from 40 to 400 Å, are formed. It has been reported that internal pressure inside the pores, built up by gas generation in the initial stage of pyrolysis of polymers, increases the pore size and volume.[49,50] In our system, the expansion of pores should be due to the evolution of dimethylamine ($HNMe_2$) and ammonia (NH_3) arising from the ammonolysis and condensation reactions among NH_3, $Si-NMe_2$, $Si-NH_2$, and Si−NH groups as shown in the IR analysis. On the other hand, chemical reactions among these functional groups attached to the pore internal surface will generate attractive forces that bring about viscous flow of the polymer and consequent shrinkage of the pores and therefore reduction of effective surface area (from 301 to 233 $m^2\ g^{-1}$).[51] Since the product pyrolyzed at 600 °C contains a considerable number of Si−NH groups, the reaction between them will release H_2 during further heating to 1000 °C and will result in viscous flow of the intermediates and shrinkage of the pores. In smaller pores (27−40 Å), the distance between Si−NH groups is so short that the reaction between them will result in elimination of the pores and loss of surface area (from 233 to 163 $m^2\ g^{-1}$). The reaction of Si−NH groups can also happen in larger pores but at an adjacent area of internal surface, which will result in progressive condensation.[51] The formation of pores at 40−100 Å is most likely due to this progressive condensation during conversion of the intermediate into the final ceramic product **3**.

Conclusion

In summary, novel dimeric titanium silylamide precursor, i.e., bis(dimethylamino)silylamino-μ-bis[(dimethylamino)-silylimino]titanium $\{Ti[NHSi(NMe_2)_3]_2[\mu\text{-}NSi(NMe_2)_3]\}_2$, **1,** has been prepared by a reaction of titanium chloride ($TiCl_4$) with lithium tris(dimethylamino)silylamide $LiHNSi(NMe_2)_3$. The successful preparation of a high surface area mesoporous silicon titanium imide, i.e., $Si_3Ti(N)(NH)_x(NH_2)_y(NMe_2)_z$, from the ammonolysis of **1** in an autoclave provides a new chemical route to multinary silicon-based imide ceramic powders. A first example of mesoporous silicon titanium nitride was obtained by pyrolysis of the silicon titanium imide at 1000 °C. The high surface area and narrow pore size distribution of the composite material open up a number of potential applications including the use of this novel mesoporous ceramic material in catalysis and filters for selective gas separation.

Acknowledgment. Part of this work was carried out as part of the EU project NANOSENSOFLEX. We also thank the Engineering and Physical Sciences Research Council (EPSRC) for financial support and the CCLRC for access to synchrotron and computing facilities at Daresbury.

Supporting Information Available: CIF data for $C_{36}H_{112}N_{24}Si_6Ti_2$. This material is available free of charge via the Internet at http://pubs.acs.org.

CM051401M

(49) Konetschny, C.; Galusek, D.; Reschke, S.; Fasel, C.; Riedel, R. *J. Eur. Ceram. Soc.* **1999**, *19*, 2789.
(50) Seitz, J.; Bill, J. *J. Mater. Sci. Lett.* **1996**, *15*, 391.
(51) Wan, J. M.; Gasch, J.; Mukherjee, A. K. *J. Am. Ceram. Soc.* **2001**, *84*, 2165.